Ag−Polymer nanocomposites for capture, detection, and destruction of bacteria

Gong, Haiyue; Zhang, Ka; Dicko, Cedric; Buelow, Leif; Ye, Lei

Published in:
ACS Applied Nano Materials

DOI:
10.1021/acsanm.9b00112

2019

Document Version:
Publisher's PDF, also known as Version of record

ACS APPLIED NANO MATERIALS

Article

Cite This: ACS Appl. Nano Mater. 2019, 2, 1655−1663

www.acsanm.org

Ag−Polymer Nanocomposites for Capture, Detection, and Destruction of Bacteria

Haiyue Gong, Ka Zhang, Cedric Dicko, Leif Bülow, and Lei Ye*

Division of Pure and Applied Biochemistry, Department of Chemistry, Lund University, Box 124, 221 00 Lund, Sweden

Supporting Information

ABSTRACT: Bacterial infection is one of the major problems for human health. To prevent outbreak of bacteria-caused diseases, early diagnosis of bacterial pathogen and effective destruction of pathogenic microorganisms are in urgent need. In this work, we developed a new multifunctional nanocomposite material that can effectively capture and destroy bacteria. Epoxide-modified nanoparticles were synthesized by microemulsion polymerization and precipitation polymerization. The epoxide groups on the particle surface were reacted with polyethylenimine to introduce cationic amine groups. The amine groups on the nanoparticle surface enhanced the colloidal stability of the particles' suspension and provided multivalent interactions to bind and destroy the bacteria. After further modification with Ag nanoparticles, the final composite nanomaterial was able to not only capture and destroy Gram-negative bacteria but also allow the bacteria's fingerprint spectra to be obtained through surface-enhanced Raman scattering. The multifunctional nanoparticles developed in this work offer a new approach toward fast capture, detection, and destruction of pathogenic bacteria.

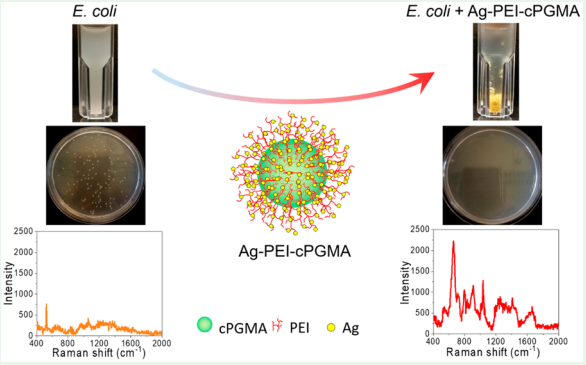

KEYWORDS: *Raman enhancement, Ag nanoparticles, nanocomposites, antibacterial, polymer nanoparticles, polyethylenimine*

1. INTRODUCTION

Bacteria are always an enormous threat to public health and security.[1] On an international level the number of antibiotic-resistant bacteria has continued to increase, which presents life-threatening challenges for medical treatment, causing significant increase in private and societal expenses.[2] To prevent an outbreak of bacteria-caused diseases, early diagnosis of bacterial pathogen and effective destruction of pathogenic microorganisms are in urgent need. For diagnosis of bacterial infection, the traditional methods are based on cultivation of bacteria in selective media followed by morphological analysis of bacterial colonies and immunological analysis of bacterial metabolites.[3] These bacteriology methods require long cultivation time (up to several days) and tedious analytical steps, which must be performed by skilled personnel in specialized laboratories.[4] More recently, some molecular methods, such as multilocus sequence typing (MLST),[5] enzyme-linked immunosorbent assay (ELISA),[6] pulsed-field gel electrophoresis (PFGE),[7] and polymerase chain reaction (PCR),[8] have shortened the time for identifying bacteria; however, these methods require expensive regents, complex procedures, and bulky laboratory instruments and produce sometimes false-positive results.[1] Therefore, new analytical techniques that can identify pathogens based on their structural characteristics and molecular fingerprint signals need to be explored.

As one of the most promising techniques, biosensor offers new possibilities for rapid and sensitive identification of bacterial pathogens. Biosensing technologies based on colorimetric, light-scattering, fluorescence, electrochemical, and surface-enhanced Raman scattering (SERS) methods have been reported for bacteria detection.[9−13] In particular, SERS has emerged as a very attractive technique for fast and selective bacterial identification, as this cost-effective method allows direct measurement of spectroscopic signals from bacteria.[14,15] Compared with label-based analytical techniques, label-free SERS is more convenient to use because it can measure directly the intrinsic vibrational fingerprint signals of bacteria, if the bacteria are placed close to or attached on nanostructured noble metals (mainly Au and Ag).[16,17] Generally speaking, three methods have been used to obtain SERS spectra from bacteria:[18] the first is to form colloidal Ag on the surface of bacteria or inside bacterial cells,[19,20] the second to place bacteria directly on a SERS substrate,[21,22] and the last to mix bacteria with colloidal Ag followed by placing the mixture on a planar surface.[23−25] Although Ag nanoparticles have intrinsic antibacterial activity, the nanoparticles themselves cannot bind bacteria rapidly if they are not properly modified with appropriate ligands.[18] Also, when dispersed in water, bare Ag nanoparticles tend to form aggregates, which reduces their colloidal stability and antibacterial activity.[26,27] These draw-

Received: January 19, 2019
Accepted: February 21, 2019
Published: February 21, 2019

DOI: 10.1021/acsanm.9b00112
ACS Appl. Nano Mater. 2019, 2, 1655−1663

backs can be overcome by anchoring Ag nanoparticles on a suitable supporting material.[26,28]

To combat pathogenic microorganisms, new antimicrobial materials are being continuously developed. Recently, Hu et al. provided a detailed review on supramolecular hydrogels for antimicrobial therapy. Because of their tunable and reversible supramolecular interactions and incorporation of various therapeutic agents (e.g., antimicrobial peptides, antibiotics, and Ag nanoparticles), the antimicrobial hydrogels exhibited unprecedented efficacy in medical applications.[29] The introduction of Ag nanoparticles can contribute to increasing antibacterial activity by releasing silver ions.[30]

The aim of this work was to develop a new type of multifunctional nanoparticles that can be used to capture, detect, and destroy Gram-negative bacteria. To realize these three functions with a single nanoparticle material, we selected to use a cationic polymer and metallic Ag to modify uniform nanoparticle scaffold. The new composite nanoparticles were expected to form strong ionic interaction with bacteria and exhibit effective bacteria-killing due to the antibacterial activities of the cationic polymer and the surface-bound Ag nanoparticles. In addition to capture and destruction of bacteria, the Ag nanoparticles were expected to make the bacteria's Raman signals become observable through surface enhanced Raman scattering. Thus, the new nanocomposite material should make it possible to achieve fast and simultaneous capture, detection, and destruction of Gram-negative bacteria.

2. EXPERIMENTAL SECTION

2.1. Materials. *N*-Isopropylacrylamide (NIPAm) was purchased from Monomer-Polymer Laboratories (Windham, NH). Methacrylic acid (MAA, 98.5%) was supplied by ACROS (Geel, Belgium). *N*,*N*′-Methylenebis(acrylamide) (Bis) was purchased from ICN Biomedicals Inc. (Warrendale, PA). Trimethylolpropane trimethacrylate (TRIM, technical grade), glycidyl methacrylate (GMA), nitrilotriacetic acid (NTA), cerium ammonium nitrate (CAN), polyethylenimine (PEI), $AgNO_3$, $NaBH_4$, and acetonitrile were purchased from Sigma-Aldrich and used without further purification. (*R*,*S*)-Propranolol hydrochloride (99%) was purchased from Fluka (Dorset, UK). Azobis(isobutyronitrile) (98%) was purchased from Merck (Darmstadt, Germany) and was recrystallized from methanol before use. Octyltrimethylammonium bromide (OTAB) was purchased from Tokyo Chemical Industry (TCI). Ultrapure water (18.2 MΩ·cm) was obtained from an ELGA LabWater System (Vivendi Water Systems Ltd.).

2.2. Culture of *E. coli*. Gram-negative *E. coli* (TG1) was cultured in LB medium at 37 °C and shaken at 160 rpm for 7 h until the optical density of the culture medium reached 1.8 at 600 nm. The cells were harvested by centrifugation at 4000 rpm (4356 *g*) for 10 min. The harvested cells were washed three times with 0.85% NaCl solution. After washing, the cells were resuspended in 0.85% NaCl solution to give an optical density of 1.7 at 600 nm, equivalent to a bacteria concentration of 1.22×10^9 CFU/mL.

2.3. Preparation of Poly(glycidyl methacrylate) Nanoparticles. Poly(glycidyl methacrylate) nanoparticles were synthesized using a previously reported method.[31] OTAB (2 g) was dissolved in 20 mL of ultrapure water and stirred at 300 rpm overnight for micelle formation. After addition of CAN (0.33 g) and NTA (0.03 g), the mixture was stirred for 30 min. Subsequently, GMA (0.5 g) was slowly added into the stirred mixture and let to react for 5 h. After the polymerization, the reaction mixture was filtered through a qualitative filter paper. The surfactant and initiators were removed with an excessive amount of ethanol. Finally, the poly(glycidyl methacrylate) nanoparticles were resuspended in water to give a concentration of 10 mg/mL. This nanoparticle product was named as PGMA. The monomer conversion was 26%.

2.4. Preparation of Cross-Linked Core−Shell Nanoparticles. The cross-linked core−shell nanoparticles were synthesized by a two-step precipitation polymerization as reported in a previous publication.[32] In the first step, the core particles were obtained by copolymerization of TRIM and MAA in acetonitrile. To control the particle size, propranolol was added in the reaction mixture. In the second step, a thin layer of copolymer shell was grafted on the core particles by copolymerization of GMA, NIPAm, and Bis.[32] This nanoparticle product was named as cPGMA. The monomer conversion was 61%.

2.5. Synthesis of PEI-Modified Nanoparticles (PEI-PGMA and PEI-cPGMA). PEI solution (1 mL, containing 100 mg of PEI) was added into 10 mL of nanoparticle suspension (containing 50 mg of PGMA or cPGMA). The mixture was stirred at 70 °C for 24 h. After the reaction, the particles were isolated by centrifugation at 4000 rpm (4356 *g*) and washed three times in water. Finally, the modified nanoparticles were suspended in water to give a concentration of 5 mg/mL. PEI with different molecular weights (M_w 800 and 25000) was used to modify the PGMA and cPGMA nanoparticles. The nanoparticles modified with the low molecular weight PEI (M_w 800) were named as 800PEI-PGMA and 800PEI-cPGMA, and the nanoparticles modified with the high molecular weight PEI (M_w 25000) were named as PEI-PGMA and PEI-cPGMA.

2.6. Synthesis of Ag-Modified Composite Nanoparticles. Ag nanoparticles were deposited on the surface of the PEI-modified nanoparticles (PEI-PGMA and PEI-cPGMA) using a previously published procedure.[33] $AgNO_3$ solution (1 mL, containing 8 mg of $AgNO_3$) was added into 10 mL of PEI-modified nanoparticle suspension (containing 15 mg of PEI-modified nanoparticles). After the mixture was stirred for 0.5 h, $NaBH_4$ (0.5 mg) dissolved in 1 mL of water was added, and the reaction mixture was stirred for 5 h at room temperature. The obtained composite particles were isolated by centrifugation (4000 rpm, 4356 *g*) and resuspended in water to give a particle concentration of 6 mg/mL. The final products were named as Ag-PEI-PGMA and Ag-PEI-cPGMA.

2.7. Antibacterial Activity Assay. *E. coli* sample (OD_{600} = 1.7) was mixed with an equal volume of 0.85% NaCl solution containing the different nanoparticles (1 mg/mL PGMA, 1 mg/mL cPGMA, 1 mg/mL PEI-PGMA, 1 mg/mL PEI-cPGMA, 2 mg/mL Ag-PEI-PGMA, 2 mg/mL Ag-PEI-cPGMA). After the samples were left on the bench for 1 h, 1 mL of liquid was taken from the upper volume and was diluted 10^6 times. The remaining volume (1 mL) was also diluted 10^6 times. From the diluted samples, 200 μL was transferred to agar plates and spread. The plates were then cultured at 37 °C for 16 h before the bacterial colonies were counted.

2.8. Raman Measurement. *E. coli* (OD_{600} = 1.7) was mixed with an equal volume of Ag-PEI-PGMA or Ag-PEI-cPGMA nanoparticles (2 mg/mL). The sample was left to stand for 1 h before the supernatant was removed. Alternatively, *E. coli*, Ag-PEI-PGMA, and Ag-PEI-cPGMA were collected separately by centrifugation. All the samples were vacuum-dried before the analytical measurement. Raman measurements were performed using an iRaman system from B&W Tek, Inc., equipped with an excitation laser at 785 nm and a source power of 325 mW. The probe was maintained at 6 mm from the sample surface. The spectra were background subtracted using Fityk software and smoothed using the Savitzky−Golay method.

2.9. Characterization. The functional groups on the polymer particles were analyzed by a Thermo Fisher-Scientific FT-IR instrument (Thermo Fisher-Scientific Inc., Waltham, MA). The ζ-potential of the particles was measured by dynamic light scattering (DLS) using a temperature-controlled particle size analyzer (Zetasizer Nano ZS, Malvern Instruments, UK). To monitor the colloidal stability of *E. coli* cells and their mixture with the composite nanoparticles, the absorbance of visible light at 600 nm of the different suspensions was recorded over 60 min using a UV−vis spectrophotometer (Cary 60 UV−vis, Agilent Technologies, US). The concentration of *E. coli* cells corresponded to OD_{600} = 1.7. The concentration of the nanoparticles was 1 mg/mL for PGMA, cPGMA, PEI-PGMA, and PEI-cPGMA and 2 mg/mL for Ag-PEI-PGMA and Ag-PEI-cPGMA. Electron microscopy imaging was performed with a JEOL scanning electron microscope

DOI: 10.1021/acsanm.9b00112
ACS Appl. Nano Mater. 2019, 2, 1655−1663

Scheme 1. Preparation of Ag−Polymer Nanocomposites Ag-PEI-PGMA (a) and Ag-PEI-cPGMA (b) Using Reaction Scheme (c)

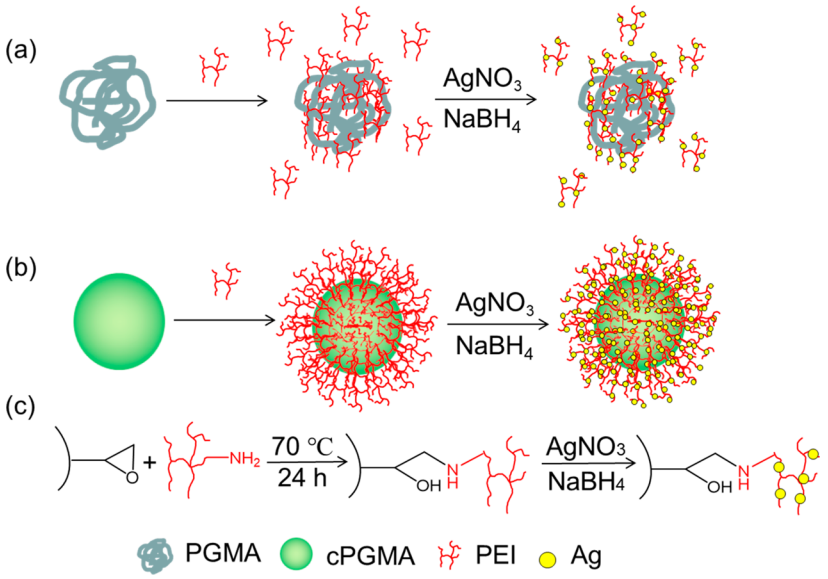

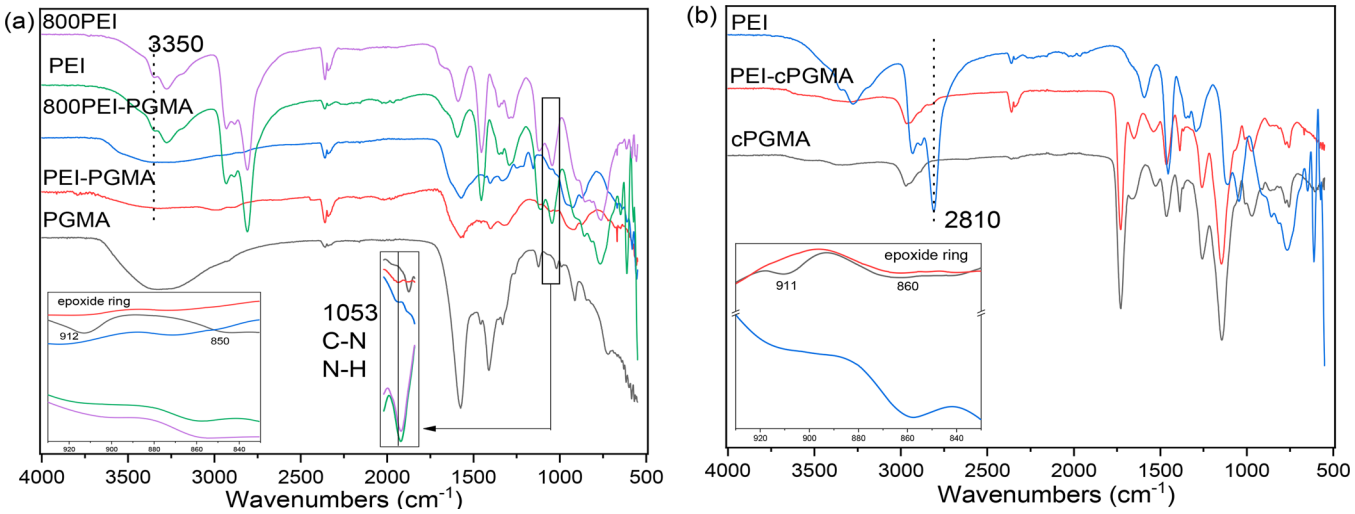

Figure 1. FT-IR spectra of PGMA and modified PGMA particles (a) and cPGMA and modified cPGMA particles (b). 800PEI stands for PEI with molecular weight of 800, and PEI stands for PEI with molecular weight of 25000.

(SEM, JSM-6700F, JEOL, Japan) and a transmission electron microscope (TEM, Tecnai Spirit BioTWIN, FEI Company, Hillsboro, OR).

3. RESULTS AND DISCUSSION

The multifunctional nanocomposite was constructed from a general-purpose nanoparticle scaffold by conjugating polyethylenimine (PEI) followed by in situ formation of Ag nanoparticles (Scheme 1). Two types of nanoparticle scaffolds containing epoxide groups were synthesized: one by microemulsion polymerization to give poly(glycidyl methacrylate) colloids and the other one by precipitation polymerization to give cross-linked organic nanoparticles bearing an epoxide-rich, soft shell. Cationic PEI was conjugated to the nanoparticle scaffolds to enhance their colloidal stability and to increase their affinity toward Gram-negative bacteria.[34] In addition, the use of PEI was also based on its proven antibacterial property and its capability to stabilize Ag nanoparticles that were synthesized on the nanocomposite surface.[33,35,36] In this design, the Ag nanoparticles were expected not only to destroy bacteria but also to enable the bound bacteria to generate detectable SERS signal.

3.1. Synthesis and Characterization of Nanoparticles.

In this work, we synthesized linear polymer nanoparticles (PGMA) and cross-linked core−shell nanoparticles (cPGMA) that both contained epoxide groups on the particle surface. In Figure 1a, after the reaction between PGMA particles and PEI, the epoxide IR bands at 912 and 850 cm^{-1} became much weaker, and the N−H stretching band at 3350 cm^{-1} disappeared. Therefore, the majority of the epoxide groups had reacted with PEI. From PEI-PGMA particles, a small band at 1053 cm^{-1} appeared. This band originated from the N−H and C−N in PEI, suggesting that PEI had reacted with PGMA particles. Comparing the IR spectra of 800PEI-PGMA with PGMA and 800PEI led to the same conclusion. For the cPGMA particles, Figure 1b shows that the epoxide bands at 911 and 860 cm^{-1} disappeared, indicating the successful conjugation of PEI to the cPGMA particles.[32] From PEI-cPGMA particles, a new band at 2810 cm^{-1} originating from PEI appeared, also confirming the reaction between cPGMA and PEI.

DOI: 10.1021/acsanm.9b00112
ACS Appl. Nano Mater. 2019, 2, 1655−1663

The UV−vis absorption spectra of PEI-PGMA and PEI-cPGMA particles, with and without Ag modification, are shown in Figure 2. As reference samples, neither $AgNO_3$ nor particles

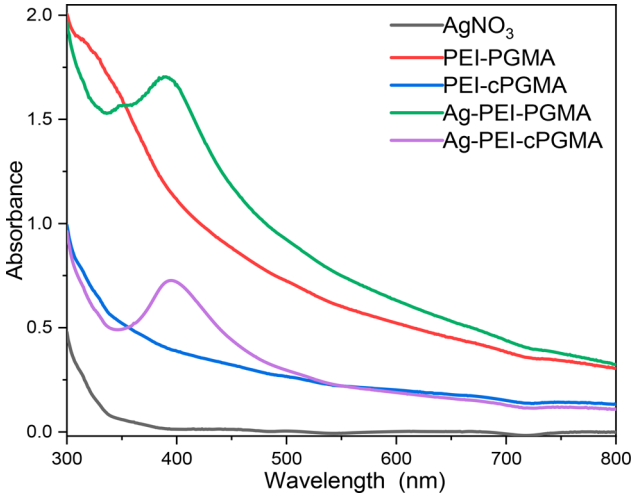

Figure 2. UV spectra of particles with and without Ag modification. The particle concentration was 0.1 mg/mL, and the concentration of $AgNO_3$ was 1 mg/mL.

before Ag modification displayed plasmon absorbance. After PEI-PGMA and PEI-cPGMA particles were modified with Ag by in situ reduction using $NaBH_4$, plasmon bands can be easily observed from Ag-PEI-PGMA and Ag-PEI-cPGMA particles. The formation of surface-deposited Ag nanoparticles is most likely mediated by PEI, as the branched amine polymer is known to bind Ag nanoparticles with a high affinity. Using PEI-PGMA or PEI-cPGMA as supporting particles, the Ag plasmon band appeared at around 400 nm, indicating that the Ag nanoparticles are spherical and had similar particle size (~10 nm).[33]

The ζ-potential of *E. coli* cells and the different nanoparticles were measured by DLS in water. The results are listed in Table 1.

Table 1. ζ-Potential of Nanoparticles Measured in Water at 20 °C by DLS

sample	ζ-potential (mV)
E. coli	−14.1 ± 0.9
PGMA	0.6 ± 0.2
800PEI-PGMA	0.6 ± 0.4
PEI-PGMA	18.7 ± 0.9
Ag-800PEI-PGMA	18.6 ± 0.6
Ag-PEI-PGMA	28.5 ± 1.1
Ag-800PEI	20.9 ± 0.5
Ag-PEI	34.2 ± 4.1
cPGMA	1.5 ± 0.2
PEI-cPGMA	22.3 ± 1.2
Ag-PEI-cPGMA	39.8 ± 6.2

The *E. coli* cells were negatively charged and had a ζ-potential of −14.1 mV. PGMA and cPGMA particles were neutral. After the introduction of high molecular weight PEI, both PEI-PGMA and PEI-cPGMA particles became positively charged. Before modification with Ag, some of the amine groups in PEI may form hydrogen bond with hydroxyl and carbonyl groups in PGMA and cPGMA, making the PEI chains less exposed on surface. After modification with Ag, the amine groups in PEI formed coordination structures with Ag nanoparticles, leading to more PEI chains to relocate on the surface. Therefore, the ζ-potential of Ag-PEI-PGMA particles increased to 28.5 mV, which was lower than Ag-PEI (34.2 mV). When low molecular weight PEI (M_w 800) was used to modify PGMA particles, the ζ-potential of the modified PGMA particles did not change, and the obtained 800PEI-PGMA particles displayed a poor colloidal stability compared with PEI-PGMA (Figure S1). Therefore, in the remaining experiments, we focused on PGMA and cPGMA nanoparticles that were modified with high molecular weight PEI (M_w 25000).

The morphology and fine structure of the nanocomposites were investigated by SEM and TEM (Figure 3). From the SEM images we can see that both the PGMA and cPGMA particles

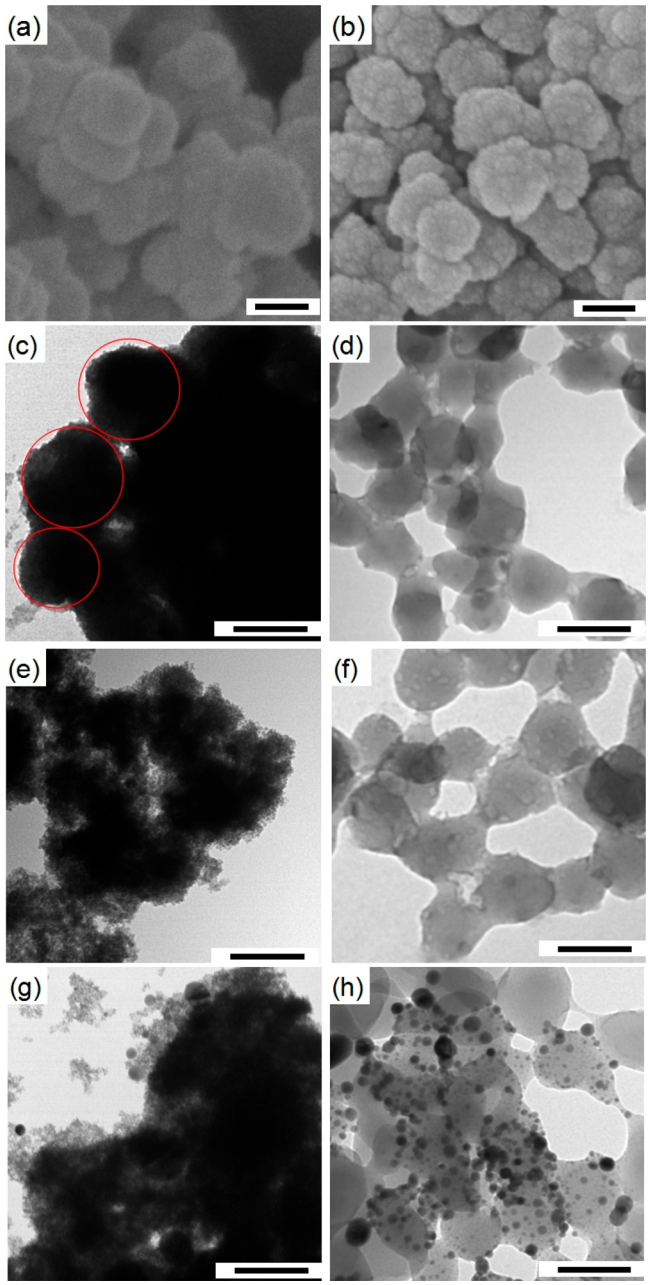

Figure 3. Electron microscope images of PGMA (a, c), cPGMA (b, d), PEI-PGMA (e), PEI-cPGMA (f), Ag-PEI-PGMA (g), and Ag-PEI-cPGMA (h). The scale bar in the SEM images (a, b) and the TEM images (c−h) is 100 nm.

DOI: 10.1021/acsanm.9b00112
ACS Appl. Nano Mater. 2019, 2, 1655−1663

had a diameter of around 100 nm (Figure 3a,b). Figure 3c is the TEM image of PGMA nanoparticles. Because these nanoparticles were hydrophobic and were not cross-linked, they appeared as large aggregates in the TEM image. The red circles in Figure 3c highlight three nanoparticles that could be distinguished. The particle size was estimated to be ~150 nm. After modification with PEI, the particles became positively charged and were much less aggregated. As a result, the individual PEI-PGMA particles could be easily recognized (Figure 3e). The PEI polymer was distinguished from the darker PGMA nanoparticles, and some PEI chains were trapped in the PGMA nanoparticles. After reducing $AgNO_3$ directly on the PEI-PGMA surface, Ag nanoparticles appeared, as can be seen in Figure 3g.

The same modification methods were repeated for modification of cPGMA nanoparticles. The major difference was that the cPGMA particles had a densely cross-linked core and a loosely cross-linked PGMA layer. After treatment with PEI, the obtained PEI-cPGMA remained as nonaggregated, separate nanoparticles (Figure 3f). In Figure 3h, the Ag nanoparticles formed on the PEI-cPGMA surface were more distinct and easily recognized. Although the size of the Ag nanoparticles was not very uniform, most of the Ag nanoparticles were found to be ~10 nm.

To understand the structure of the different particles in water, we also measured the hydrodynamic size of the particles using DLS (Table 2). Although PGMA and cPGMA exhibited similar size under SEM (Figure 3a,b), the hydrodynamic diameter of PGMA (329 nm) is much larger than cPGMA (182 nm). The reason is that PGMA particle is composed of a linear polymer, which can be hydrated to a larger extent than cPGMA particle. For cPGMA particle, hydration takes place mainly in the particle shell. After introduction of PEI, the hydrodynamic size of PEI-PGMA and PEI-cPGMA increased to 399 and 232 nm, respectively. After the final modification with Ag, the hydrodynamic particle size of Ag-PEI-PGMA increased to 431 nm. The hydrodynamic size of Ag-PEI-cPGMA particles could not be determined due to their fast sedimentation during the DLS measurement.

Table 2. Hydrodynamic Size of Nanoparticles Measured by DLS in Water at 20 °C

sample	diameter (nm)
PGMA	329.4 ± 8.8
PEI-PGMA	399.2 ± 7.6
Ag-PEI-PGMA	430.9 ± 11.6
cPGMA	181.8 ± 1.9
PEI-cPGMA	232.5 ± 12.5

3.2. Capturing *E. coli* Using PEI-Modified Nanoparticles. On the basis of the fact that the PEI-modified nanoparticles (PEI-PGMA and PEI-cPGMA) had multiple amine groups on their surface, we expected that these particles can bind negatively charged bacteria and cause the bacteria to be quickly separated from water by simple sedimentation. To test our hypothesis, we first studied the colloidal stability of *E. coli* cells before and after addition of the different nanoparticles. The colloidal stability was investigated by measuring the change of light absorption/scattering of cellular and particle suspensions over a 1 h period. As shown in Figure 4a, *E. coli* itself remains as a stable suspension. After addition of the positively charged composite nanoparticles (PEI-PGMA and Ag-PEI-PGMA), the bacterial cells settled rapidly due to their adsorption to the composite nanoparticles. In a similar manner, in Figure 4b, the originally stable *E. coli* cells precipitated rapidly after addition of the positively charged nanoparticles PEI-cPGMA and Ag-PEI-cPGMA. In the absence of *E. coli*, PEI-PGMA and PEI-cPGMA exhibited similar sedimentation rates. However, in the presence of *E. coli* the situation became different. According to Figure 4b, PEI-cPGMA can form cross-linked particle aggregates with *E. coli* cells more efficiently and thereby precipitate more quickly than PEI-PGMA. The stronger interaction of PEI-cPGMA with *E. coli* cells may be explained in part by its higher ζ-potential and in part by its different size and structure compared to PEI-PGMA. In fact, only the two PEI-modified core−shell nanoparticles, PEI-cPGMA and Ag-PEI-cPGMA, had the fastest sedimentation rate of *E. coli*. Under the experimental conditions, the bacterial cells were settled to the bottom by these two nanocomposites within 1 min (Figure 4b). Before Ag modification, both PEI-PGMA and PEI-cPGMA remained as stable suspensions in 3600 s. The introduction of Ag caused Ag-

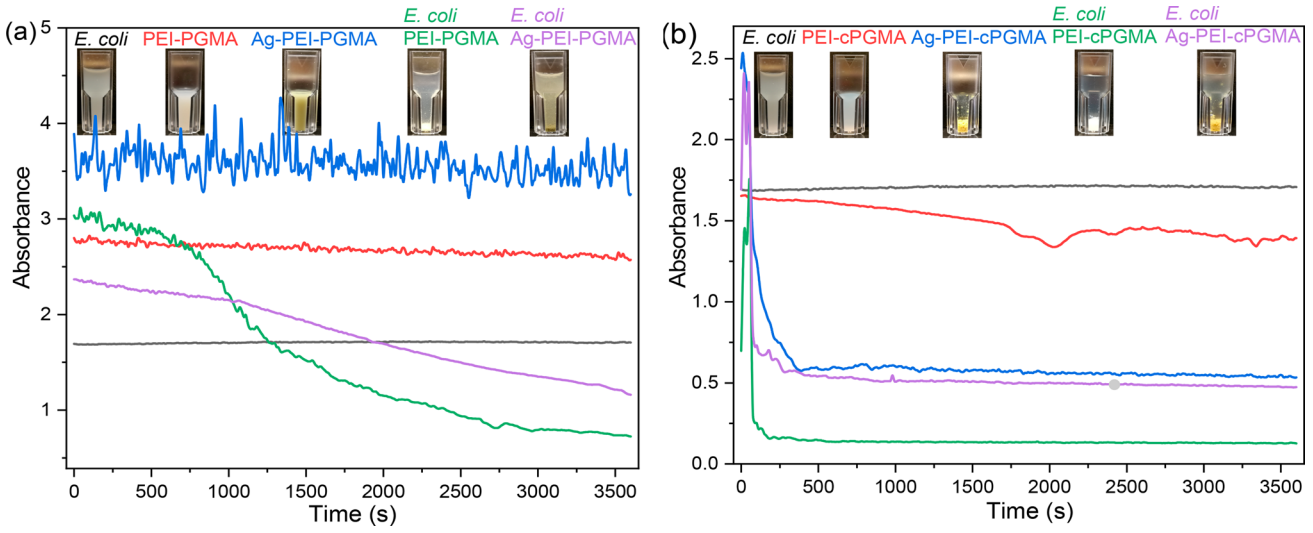

Figure 4. Colloidal stability of *E. coli* cells before and after addition of different nanoparticles. Light absorbance at 600 nm wavelength was monitored over a 1 h period.

DOI: 10.1021/acsanm.9b00112
ACS Appl. Nano Mater. 2019, 2, 1655−1663

PEI-cPGMA particles to settle to the bottom in only a few minutes. In contrast, the Ag-PEI-PGMA suspension was stable in 3600 s. The different colloidal stability between Ag-PEI-PGMA and Ag-PEI-cPGMA can be explained as follows: due to its linear structure, PGMA has a lower density than cPGMA. Therefore, Ag-PEI-PGMA can be stabilized more easily via the electrostatic repulsion. For the suspension of Ag-PEI-cPGMA, the optical absorbance observed after 1 h remained constant. The remaining absorbance was caused by a small amount of PEI-cPGMA particles rather than free Ag nanoparticles because a UV scan of the supernatant from the same sample did not show the characteristic plasmon band for Ag nanoparticles (Figure S2). Note that without Ag-PEI-cPGMA *E. coli* remained stable in suspension, and the bacterial suspension gave a constant absorbance value of 1.7 for 1 h. After addition of Ag-PEI-cPGMA, the bacterial cells bound to the particles and settled quickly. As a result, the absorbance value decreased quickly to 0.5, which is even lower than the absorbance value contributed from the supernatant of Ag-PEI-cPGMA (Figure 4b). The fast sedimentation of *E. coli* in the presence of Ag-PEI-cPGMA can only be explained as a result of strong interaction between *E. coli* and Ag-PEI-cPGMA particles.

More detailed structure of the particle-mediated *E. coli* aggregates was inspected using TEM (Figure 5). When PGMA and cPGMA nanoparticles were added to *E. coli* culture, very few nanoparticles were found to be in contact with the bacterial cells (Figure 5a,b). When the PEI-modified nanoparticles (PEI-PGMA and PEI-cPGMA) were added, the positively charged nanoparticles bound readily to the *E. coli* cells to form the particle-cell aggregates (Figure 5c,d). The addition of metallic Ag in the PEI-modified nanoparticles exhibited no influence on the electrostatic interaction between the bacterial cells and the composite particles (Figure 5e,f). The inserted images in Figure 5 show the enlarged *E. coli* surface after the cells were exposed to the composite nanoparticles.

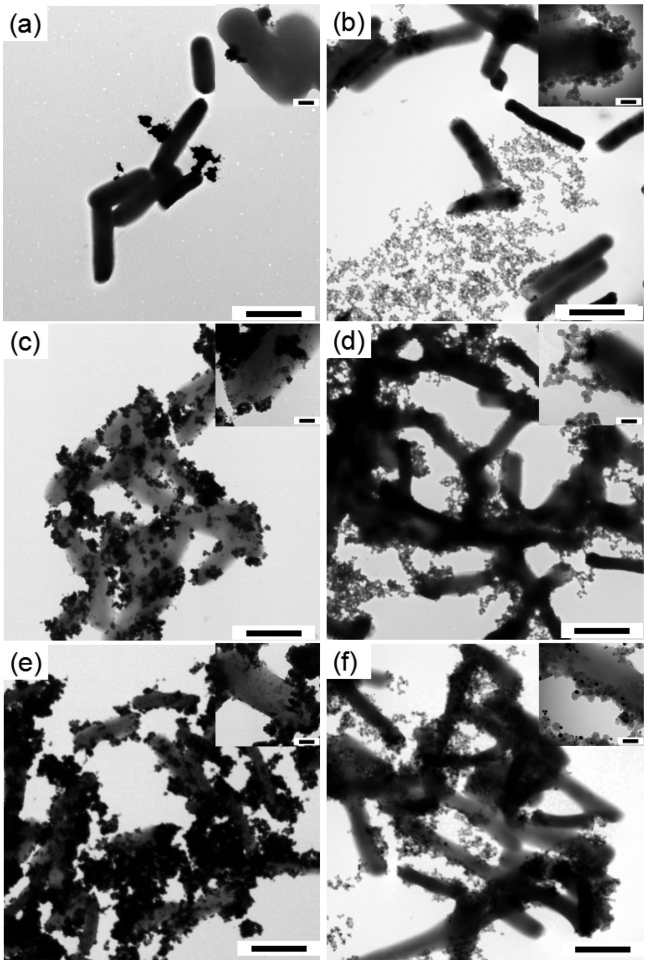

Figure 5. Left column: TEM images of *E. coli* mixed with PGMA (a), PEI-PGMA (c), and Ag-PEI-PGMA (e). Right column: TEM images of *E. coli* mixed with cPGMA (b), PEI-cPGMA (d), and Ag-PEI-cPGMA (f). The scale bar is 2 μm for the main images and 200 nm for the insets.

3.3. Destruction of Bacteria by PEI-Modified Nanoparticles. The antibacteria activities of the nanocomposites were evaluated using a colony-counting method. Figure 6a shows the agar plates containing *E. coli* cultured with and without the different PGMA-based nanoparticles. The unmodified PGMA nanoparticles exhibited only limited effect of capturing and killing the bacterial cells. After modification with PEI, the positively charged nanocomposite PEI-PGMA displayed much higher potency in capturing and destroying the bacteria. Further modification with Ag made the Ag-PEI-PGMA to become an even more effective antibacteria material. As shown in Figure S3, when the same concentration of particles was used, Ag-PEI-PGMA exhibited better antibacterial effect than PEI-PGMA. If we assume that the conversion of Ag nanoparticles was 100%, then a concentration of 1.5 mg/mL of Ag-PEI-PGMA has the same content of polymer as 1 mg/mL of PEI-PGMA. Obviously, the increased antibacterial activity was contributed by the Ag nanoparticles. For the cPGMA-based composite nanoparticles, a similar effect of surface modification with PEI and Ag in terms of bacteria capture and destruction was observed. Upon comparison of Figure 6b with Figure 6a, it is obvious that Ag-PEI-cPGMA is the most potent material for capture and destruction of *E. coli*.

The structural integrity of the antibacterial materials deserves further discussion. In the case of the PGMA-based nanoparticles, some PEI molecules seem to detach from the supporting PGMA nanoparticles, and some Ag nanoparticles could be observed in the detached PEI (Figure 3g). When the supporting nanoparticle was changed to the cross-linked cPGMA, the final antibacterial nanoparticle Ag-PEI-cPGMA became much more stable and showed no obvious release of PEI during the antibacterial experiment.

3.4. Detection of SERS Signals from *E. coli*. The presence of metallic Ag in the composite nanoparticles not only can improve the antibacterial activity but also provide a possibility toward direct detection of bacteria through their characteristic Raman signal. The SERS spectra recorded are shown in Figure 7, where the effect of the Ag-modified nanocomposites, Ag-PEI-PGMA and Ag-PEI-cPGMA, to enhance the Raman signal of *E. coli* is obvious. From the Ag-modified nanoparticles and the *E. coli* cells themselves, only a few weak Raman bands could be detected. After the *E. coli* cells were mixed with the Ag-modified nanoparticles, several Raman bands originating from the *E. coli* cells became visible: the band at 657 cm^{-1} can be assigned to guanine,[37] tyrosine,[38] and the COO^- deformation.[1] The bands at 732 and 795 cm^{-1} can be attributed to adenine[1,37−39] and cytosine,[40] and the bands at 891, 909, and 1038 cm^{-1} are more likely arising from the fatty acids[40] and the lipid layer components of the cell walls and membranes.[41] The Raman signal at 1372 cm^{-1} can be assigned to the COO^- stretching[1,38] and the CH deformation[1] in the proteins, and the band at 1620 cm^{-1} can be attributed to the amide II signal.[1] The reason that

DOI: 10.1021/acsanm.9b00112
ACS Appl. Nano Mater. 2019, 2, 1655−1663

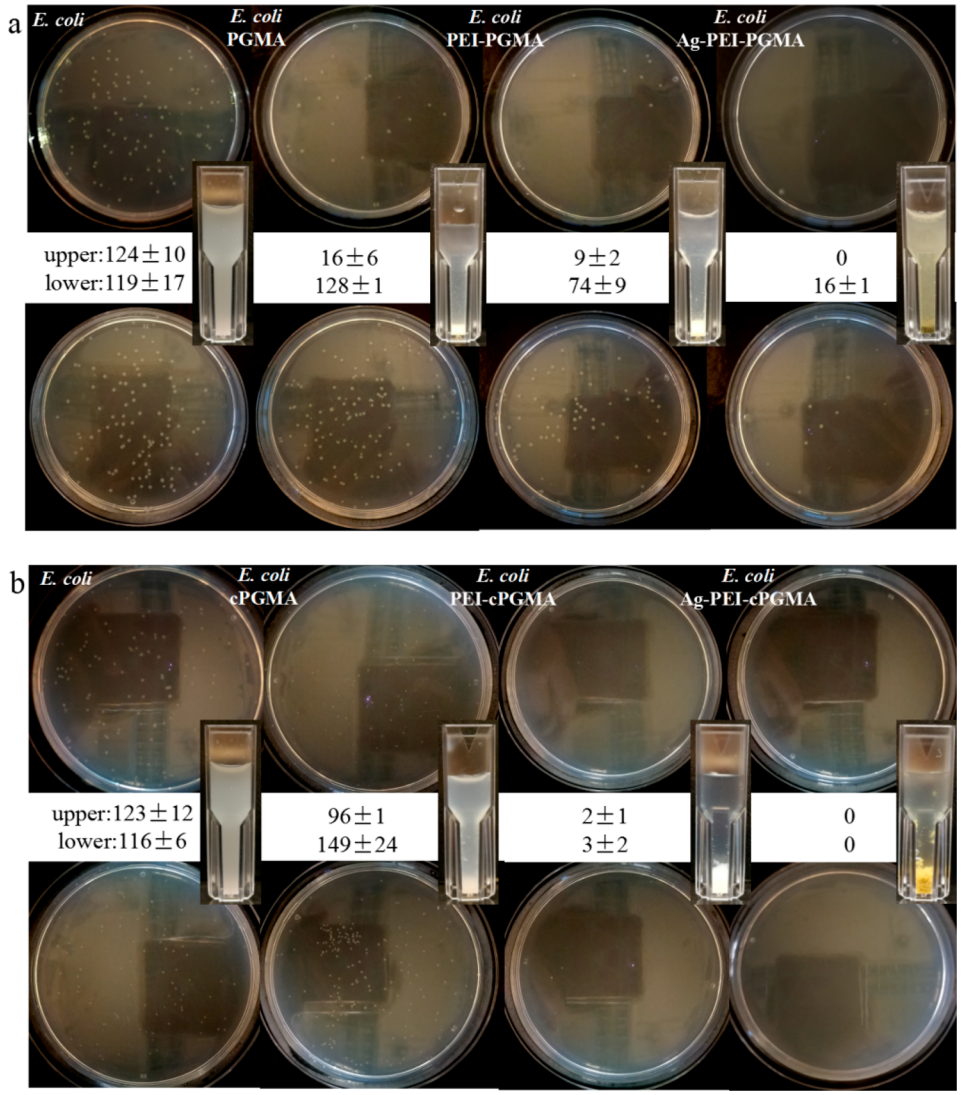

Figure 6. Photographs of agar plates of *E. coli* treated with (a) the PGMA-based nanocomposite particles and (b) the cPGMA-based nanocomposite particles. In the experiment an equal volume of nanoparticle suspension in 0.85% NaCl was added to the *E. coli* culture. The concentration of the nanoparticles was 1 mg/mL for PGMA, PEI-PGMA, cPGMA, and PEI-cPGMA and 2 mg/mL for Ag-PEI-PGMA and Ag-PEI-cPGMA. The numbers were the colony counts.

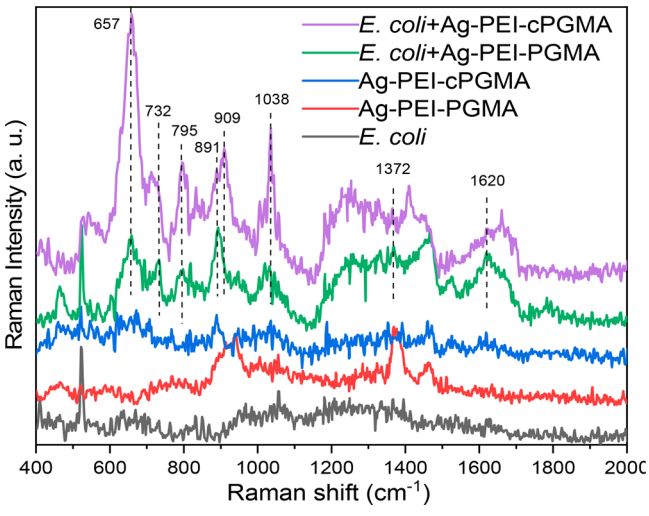

Figure 7. Raman spectra of *E. coli* and the composite nanoparticles before and after their combination.

guanine, tyrosine, adenine and cytosine generated relatively strong signals may be explained by their deposition on the bacterial outer layer as a result of degradation of nucleotides caused by the bacterial starvation response.[42] Unlike for small organic molecules, for *E. coli* it is difficult to calculate the enhancement factor of SERS. Therefore, we considered to use analytical enhancement factor (AEF) instead to estimate the effect of the surface enhancement according to the following equation:[43]

$$\mathrm{AEF} = (I_{\mathrm{SERS}}/C_{\mathrm{SERS}})/(I_{\mathrm{OR}}/C_{\mathrm{OR}}) \quad (1)$$

where I_{SERS} and I_{OR} are the signal intensities with and without the SERS and C_{SERS} and C_{OR} are the concentrations of analyte used to measure the SERS and the ordinary Raman signal, respectively. If we use the Raman band at 657 cm^{-1} as an example, the AEF of Ag-PEI-cPGMA for *E. coli* detection is 2 times higher than Ag-PEI-PGMA. Because *E. coli* itself did not generate any detectable Raman band (Figure 7, black line), it was not possible to calculate the absolute value of AEF for the two types of Ag−polymer composites. On the basis of its

DOI: 10.1021/acsanm.9b00112
ACS Appl. Nano Mater. 2019, 2, 1655−1663

stronger SERS effect, we believe that the new Ag-modified nanocomposite Ag-PEI-cPGMA can be further exploited to realize rapid detection of Gram-negative bacteria in the future.

4. CONCLUSIONS

In this work, we have prepared new multifunctional nanoparticles that enable simultaneous capture and destruction of Gram-negative bacteria *E. coli*. The Ag- and PEI-modified core−shell nanoparticles were robust and maintain a high structural integrity and could enhance the Raman signals originating from the bound bacterial cells. Using a modular synthetic approach, we have shown that cross-linked core−shell nanoparticles composed of a dense core and a more open shell structure offered the best surface modification. The multifunctional material developed in this work opens new opportunity to realizing simultaneous collection, destruction, and identification of pathogenic bacteria. We are presently studying the use of the cross-linked core of the multifunctional nanoparticles as a switchable reservoir for controlled release of antimicrobial agents. The ultimate goal is to realize smart antimicrobial materials capable of capture, destruction, and identification of pathogenic microorganisms with a high selectivity.

■ ASSOCIATED CONTENT

Supporting Information

The Supporting Information is available free of charge on the ACS Publications website at DOI: 10.1021/acsanm.9b00112.

Preparation of cross-linked core−shell nanoparticles (cPGMA), colloidal stability data of PGMA and 800PEI-PGMA nanoparticles, UV−vis spectra of particle suspension after sedimentation, and additional antimicrobial activity data (PDF)

■ AUTHOR INFORMATION

Corresponding Author

*E-mail: lei.ye@tbiokem.lth.se.

ORCID

Ka Zhang: 0000-0001-5236-4218
Cedric Dicko: 0000-0001-6377-3500
Leif Bülow: 0000-0003-4966-8610
Lei Ye: 0000-0002-3646-4072

Notes

The authors declare no competing financial interest.

■ ACKNOWLEDGMENTS

This work was supported by the Swedish Research Council FORMAS (grant 2016-00591) and the Swedish Foundation for Strategic Research (grant SM16-0024). H. Y. Gong thanks the China Scholarship Council (CSC) for a PhD fellowship.

■ REFERENCES

(1) Wang, C.; Wang, J.; Li, M.; Qu, X.; Zhang, K.; Rong, Z.; Xiao, R.; Wang, S. A Rapid SERS Method for Label-Free Bacteria Detection Using Polyethylenimine-Modified Au-Coated Magnetic Microspheres and Au@Ag Nanoparticles. *Analyst* **2016**, *141*, 6226−6238.

(2) *World Health Organization Antimicrobial Resistance: Global Report on Surveillance*; World Health Organization: 2014.

(3) Barenfanger, J.; Drake, C.; Kacich, G. Clinical and Financial Benefits of Rapid Bacterial Identification and Antimicrobial Susceptibility Testing. *J. Clin. Microbiol.* **1999**, *37*, 1415−1418.

(4) Yang, D.; Zhou, H.; Haisch, C.; Niessner, R.; Ying, Y. Reproducible *E. Coli* Detection Based on Label-Free SERS and Mapping. *Talanta* **2016**, *146*, 457−463.

(5) Enright, M. C.; Day, N. P.; Davies, C. E.; Peacock, S. J.; Spratt, B. G. Multilocus Sequence Typing for Characterization of Methicillin-Resistant and Methicillin-Susceptible Clones of *Staphylococcus Aureus*. *J. Clin. Microbiol.* **2000**, *38*, 1008−1015.

(6) Dylla, B. L.; Vetter, E. A.; Hughes, J. G.; Cockerill, F. R. Evaluation of an Immunoassay for Direct Detection of *Escherichia Coli* O157 in Stool Specimens. *J. Clin. Microbiol.* **1995**, *33*, 222−224.

(7) Blanc, D. S.; Struelens, M. J.; Deplano, A.; De Ryck, R.; Hauser, P. M.; Petignat, C.; Francioli, P. Epidemiological Validation of Pulsed-Field Gel Electrophoresis Patterns for Methicillin-Resistant *Staphylococcus Aureus*. *J. Clin. Microbiology* **2001**, *39*, 3442−3445.

(8) Belgrader, P.; Benett, W.; Hadley, D.; Richards, J.; Stratton, P.; Mariella, R.; Milanovich, F. PCR Detection of Bacteria in Seven Minutes. *Science* **1999**, *284*, 449−450.

(9) Abdelhamid, H. N.; Wu, H. F. Multifunctional Graphene Magnetic Nanosheet Decorated with Chitosan for Highly Sensitive Detection of Pathogenic Bacteria. *J. Mater. Chem. B* **2013**, *1*, 3950−3961.

(10) Cheng, D.; Yu, M.; Fu, F.; Han, W.; Li, G.; Xie, J.; Song, Y.; Swihart, M. T.; Song, E. Dual Recognition Strategy for Specific and Sensitive Detection of Bacteria Using Aptamer-Coated Magnetic Beads and Antibiotic-Capped Gold Nanoclusters. *Anal. Chem.* **2016**, *88*, 820−825.

(11) Qiu, S.; Lin, Z.; Zhou, Y.; Wang, D.; Yuan, L.; Wei, Y.; Dai, T.; Luo, L.; Chen, G. Highly Selective Colorimetric Bacteria Sensing Based on Protein-Capped Nanoparticles. *Analyst* **2015**, *140*, 1149−1154.

(12) Li, D.; Dong, Y.; Li, B.; Wu, Y.; Wang, K.; Zhang, S. Colorimetric Sensor Array with Unmodified Noble Metal Nanoparticles for Naked-Eye Detection of Proteins and Bacteria. *Analyst* **2015**, *140*, 7672−7677.

(13) Madiyar, F. R.; Bhana, S.; Swisher, L. Z.; Culbertson, C. T.; Huang, X.; Li, J. Integration of a Nanostructured Dielectrophoretic Device and a Surface-Enhanced Raman Probe for Highly Sensitive Rapid Bacteria Detection. *Nanoscale* **2015**, *7*, 3726−3736.

(14) Efrima, S.; Zeiri, L. Understanding SERS of Bacteria. *J. Raman Spectrosc.* **2009**, *40*, 277−288.

(15) Liu, T. Y.; Tsai, K. T.; Wang, H. H.; Chen, Y.; Chen, Y. H.; Chao, Y. C.; Chang, H. H.; Lin, C. H.; Wang, J. K.; Wang, Y. L. Functionalized Arrays of Raman-Enhancing Nanoparticles for Capture and Culture-Free Analysis of Bacteria in Human Blood. *Nat. Commun.* **2011**, *2*, 538.

(16) Li, J. F.; Huang, Y. F.; Ding, Y.; Yang, Z. L.; Li, S. B.; Zhou, X. S.; Fan, F. R.; Zhang, W.; Zhou, Z. Y.; Ren, B.; Wang, Z. L. Shell-Isolated Nanoparticle-Enhanced Raman Spectroscopy. *Nature* **2010**, *464*, 392−395.

(17) Wu, X.; Xu, C.; Tripp, R. A.; Huang, Y. W.; Zhao, Y. Detection and Differentiation of Foodborne Pathogenic Bacteria in Mung Bean Sprouts Using Field Deployable Label-Free SERS Devices. *Analyst* **2013**, *138*, 3005−3012.

(18) Mosier-Boss, P. A. Review on SERS of Bacteria. *Biosensors* **2017**, *7*, 51.

(19) Efrima, S.; Bronk, B. V. Silver Colloids Impregnating or Coating Bacteria. *J. Phys. Chem. B* **1998**, *102*, 5947−5950.

(20) Jarvis, R. M.; Brooker, A.; Goodacre, R. Surface-Enhanced Raman Spectroscopy for Bacterial Discrimination Utilizing a Scanning Electron Microscope with a Raman Spectroscopy Interface. *Anal. Chem.* **2004**, *76*, 5198−5202.

(21) Sanchez-Cortes, S.; García-Ramos, J. V. SERS of AMP on Different Silver Colloids. *J. Mol. Struct.* **1992**, *274*, 33−45.

(22) Stephen, K. E.; Homrighausen, D.; DePalma, G.; Nakatsu, C. H.; Irudayaraj, J. Surface Enhanced Raman Spectroscopy (SERS) for the Discrimination of *Arthrobacter* Strains Based on Variations in Cell Surface Composition. *Analyst* **2012**, *137*, 4280−4286.

(23) Zhou, H.; Yang, D.; Ivleva, N. P.; Mircescu, N. E.; Niessner, R.; Haisch, C. SERS Detection of Bacteria in Water by In Situ Coating with Ag Nanoparticles. *Anal. Chem.* **2014**, *86*, 1525−1533.

DOI: 10.1021/acsanm.9b00112
ACS Appl. Nano Mater. 2019, 2, 1655−1663

(24) Kahraman, M.; Yazıcı, M. M.; Şahin, F.; Çulha, M. Convective Assembly of Bacteria for Surface-Enhanced Raman Scattering. *Langmuir* **2008**, *24*, 894−901.
(25) Cam, D.; Keseroglu, K.; Kahraman, M.; Sahin, F.; Culha, M. Multiplex Identification of Bacteria in Bacterial Mixtures with Surface Enhanced Raman Scattering. *J. Raman Spectrosc.* **2010**, *41*, 484−489.
(26) Kellici, S.; Acord, J.; Vaughn, A.; Power, N. P.; Morgan, D. J.; Heil, T.; Facq, S. P.; Lampronti, G. I. Calixarene Assisted Rapid Synthesis of Silver-Graphene Nanocomposites with Enhanced Antibacterial Activity. *ACS Appl. Mater. Interfaces* **2016**, *8*, 19038−19046.
(27) Chen, X.; Huang, X.; Zheng, C.; Liu, Y.; Xu, T.; Liu, J. Preparation of Different Sized Nano-Silver Loaded on Functionalized Graphene Oxide with Highly Effective Antibacterial Properties. *J. Mater. Chem. B* **2015**, *3*, 7020−7029.
(28) Wang, H.; Zhou, Y.; Jiang, X.; Sun, B.; Zhu, Y.; Wang, H.; Su, Y.; He, Y. Simultaneous Capture, Detection, and Inactivation of Bacteria as Enabled by a Surface-Enhanced Raman Scattering Multifunctional Chip. *Angew. Chem., Int. Ed.* **2015**, *54*, 5132−5136.
(29) Hu, B.; Owh, C.; Chee, P. L.; Leow, W. R.; Liu, X.; Wu, Y. L.; Guo, P.; Loh, X. J.; Chen, X. Supramolecular Hydrogels for Antimicrobial Therapy. *Chem. Soc. Rev.* **2018**, *47*, 6917−6929.
(30) Xiu, Z. M.; Zhang, Q. B.; Puppala, H. L.; Colvin, V. L.; Alvarez, P. J. Negligible Particle-Specific Antibacterial Activity of Silver Nanoparticles. *Nano Lett.* **2012**, *12*, 4271−4275.
(31) Jang, J.; Bae, J.; Ko, S. Synthesis and Curing of Poly(Glycidyl Methacrylate) Nanoparticles. *J. Polym. Sci., Part A: Polym. Chem.* **2005**, *43*, 2258−2265.
(32) Gong, H.; Hajizadeh, S.; Jiang, L.; Ma, H.; Ye, L. Dynamic Assembly of Molecularly Imprinted Polymer Nanoparticles. *J. Colloid Interface Sci.* **2018**, *509*, 463−471.
(33) Mohammed, H. S.; Shipp, D. A. Uniform Sub Micron Polymer Spheres Coated with Ag Nanoparticles. *Macromol. Rapid Commun.* **2006**, *27*, 1774−1778.
(34) Yan, L.; Chang, Y. N.; Zhao, L.; Gu, Z.; Liu, X.; Tian, G.; Zhou, L.; Ren, W.; Jin, S.; Yin, W.; Chang, H.; et al. The Use of Polyethylenimine-Modified Graphene Oxide as a Nanocarrier for Transferring Hydrophobic Nanocrystals into Water to Produce Water-Dispersible Hybrids for Use in Drug Delivery. *Carbon* **2013**, *57*, 120−129.
(35) Giano, M. C.; Ibrahim, Z.; Medina, S. H.; Sarhane, K. A.; Christensen, J. M.; Yamada, Y.; Brandacher, G.; Schneider, J. P. Injectable Bioadhesive Hydrogels with Innate Antibacterial Properties. *Nat. Commun.* **2014**, *5*, 4095.
(36) Wang, X.; Wang, Y.; Bi, S.; Wang, Y.; Chen, X.; Qiu, L.; Sun, J. Optically Transparent Antibacterial Films Capable of Healing Multiple Scratches. *Adv. Funct. Mater.* **2014**, *24*, 403−411.
(37) Dina, N. E.; Zhou, H.; Colniţă, A.; Leopold, N.; Szoke-Nagy, T.; Coman, C.; Haisch, C. Rapid Single-Cell Detection and Identification of Pathogens by Using Surface-Enhanced Raman Spectroscopy. *Analyst* **2017**, *142*, 1782−1789.
(38) Kao, P.; Malvadkar, N. A.; Cetinkaya, M.; Wang, H.; Allara, D. L.; Demirel, M. C. Surface Enhanced Raman Detection on Metalized Nanostructured Poly(P-Xylylene) Films. *Adv. Mater.* **2008**, *20*, 3562−3565.
(39) Alula, M. T.; Krishnan, S.; Hendricks, N. R.; Karamchand, L.; Blackburn, J. M. Identification and Quantitation of Pathogenic Bacteria via In-Situ Formation of Silver Nanoparticles on Cell Walls, and Their Detection via SERS. *Microchim. Acta* **2017**, *184*, 219−227.
(40) De Gelder, J.; De Gussem, K.; Vandenabeele, P.; Moens, L. Reference Database of Raman Spectra of Biological Molecules. *J. Raman Spectrosc.* **2007**, *38*, 1133−1147.
(41) Premasiri, W. R.; Moir, D. T.; Klempner, M. S.; Krieger, N.; Jones, G.; Ziegler, L. D. Characterization of the Surface Enhanced Raman Scattering (SERS) of Bacteria. *J. Phys. Chem. B* **2005**, *109*, 312−320.
(42) Premasiri, W. R.; Lee, J. C.; Sauer-Budge, A.; Théberge, R.; Costello, C. E.; Ziegler, L. D. The Biochemical Origins of the Surface-Enhanced Raman Spectra of Bacteria: a Metabolomics Profiling by SERS. *Anal. Bioanal. Chem.* **2016**, *408*, 4631−4647.
(43) Bai, S.; Lin, Y. H.; Zhang, X. P.; Zhou, W. P.; Chen, T.; Ma, Y.; Hou, T. X.; Bridges, D.; Oakes, K. D.; Hu, A. Two-Step Photonic Reduction of Controlled Periodic Silver Nanostructures for Surface-Enhanced Raman Spectroscopy. *Plasmonics* **2015**, *10*, 1675−1685.

DOI: 10.1021/acsanm.9b00112
ACS Appl. Nano Mater. 2019, 2, 1655−1663

Supporting Information

Ag-Polymer Nanocomposites for Capture, Detection and Destruction of Bacteria

*Haiyue Gong, Ka Zhang, Cedric Dicko, Leif Bülow, Lei Ye**

Division of Pure and Applied Biochemistry, Department of Chemistry, Lund University, Box 124, 221 00 Lund, Sweden

,

Corresponding Author

∗Lei Ye. Tel: +46 462229560. E-mail: lei.ye@tbiokem.lth.se

Preparation of cross-linked core-shell nanoparticles (cPGMA)

The cross-linked core-shell nanoparticles were synthesized by a two-step precipitation polymerization as described in our previous publication.[1]

Step 1: A solution of propranolol (137 mg, 0.53 mmol), methacrylic acid (113 mg, 1.31 mmol) and trimethylolpropane trimethacrylate (648 mg, 2.02 mmol) was prepared in 40 mL acetonitrile in a one-neck round-bottomed flask. After addition of azobisisobutyronitrile (28 mg), the solution was purged with a gentle flow of nitrogen gas for 5 min and then sealed. The flask was attached to the rotor-arm of a rotary evaporator. The polymerization was carried out at 60 °C for 24 h while the reactor was rotated at ~30 rpm to provide a gentle agitation.

Step 2: A mixture of *N*-isopropylacrylamide (566 mg, 5 mmol), *N,N'*-methylenebisacrylamide (77.2 mg, 0.5 mmol), glycidyl methacrylate (355 mg, 2.5 mmol) and azobisisobutyronitrile (24 mg) was added into the original reaction flask. The mixture was sonicated for 3 min, then purged with nitrogen gas for 5 min. The reactor was attached to the rotor-arm of a rotary evaporator to initiate the second step polymerization for 48 h while the reactor was rotated at ~30 rpm to provide a gentle agitation. After polymerization, the polymer particles were collected by centrifugation at 12000 rpm (13680 × *g*) for 15 min. The polymer particles washed with methanol containing 10% acetic acid (v/v) until no propranolol could be detected from the washing solvent by using UV spectrometric measurement at 290 nm. The polymer particles were finally washed with acetone and dried in a vacuum desiccator.

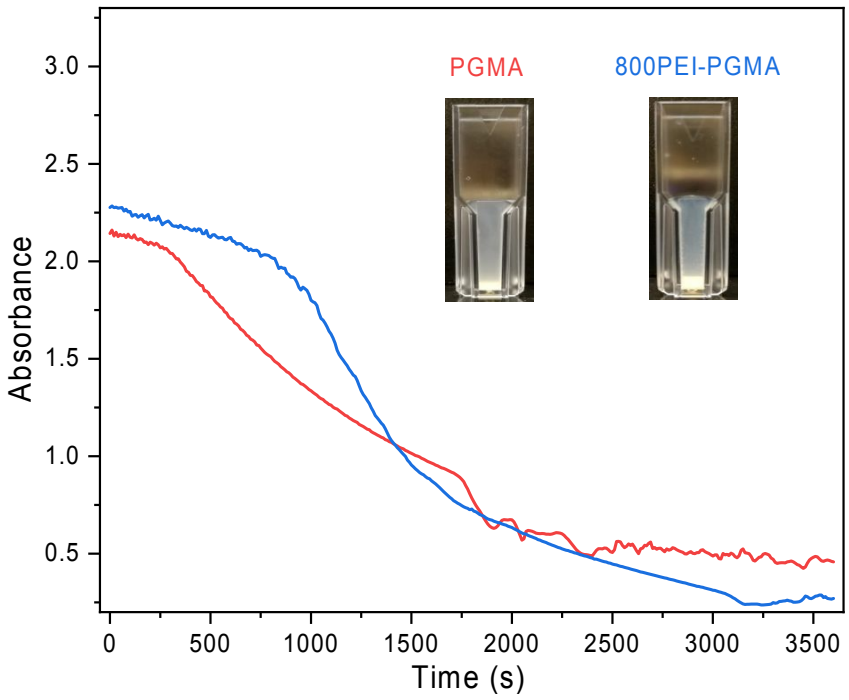

Figure S1. Colloidal stability of PGMA and 800PEI-PGMA nanoparticles. Light absorbance at 600 nm wavelength was monitored over an 1 h period.

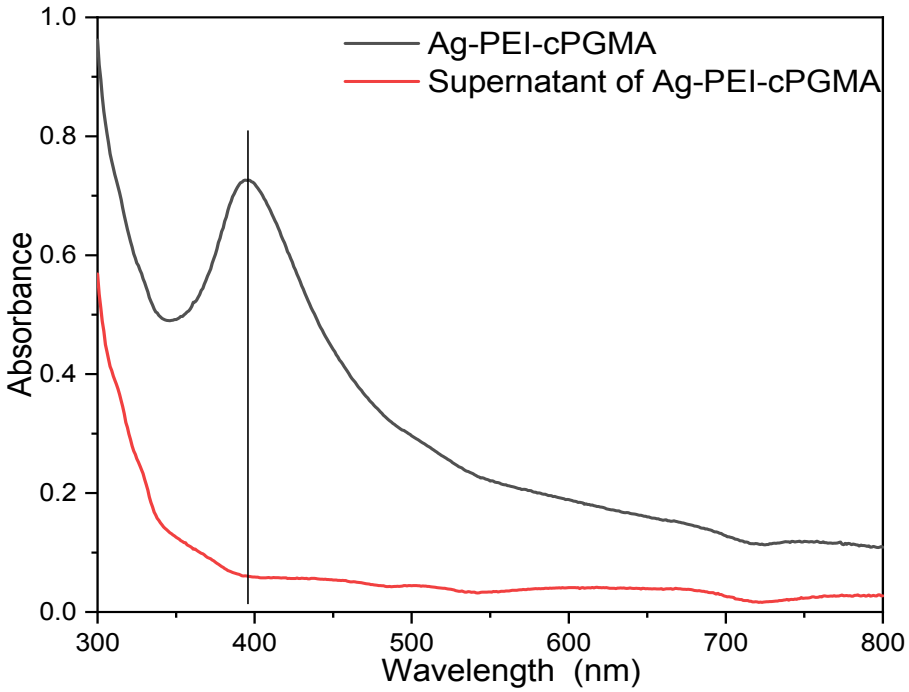

Figure S2. UV-vis spectra of Ag-PEI-cPGMA suspension collected immediately after preparation (black line), and the supernatant (red line) collected from the same sample after standing for 1 h.

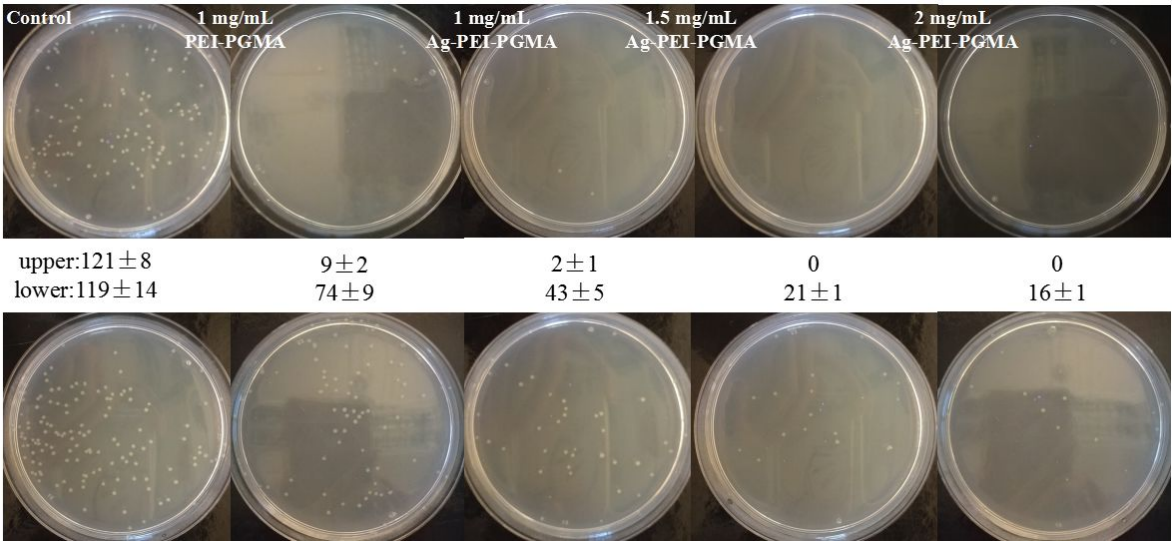

Figure S3. Photographs of agar plates of *E. coli* treated with PGMA-based nanocomposite particles. In the experiment an equal volume of nanoparticle suspension in 0.85% NaCl was added to the *E. coli* culture. In the control sample, *E. coli* was mixed with an equal volume of 0.85% NaCl. The concentration of the nanoparticles was as shown in the figure. The numbers were the colony counts.

Reference

[1] Gong, H.; Hajizadeh, S.; Jiang, L.; Ma, H.; Ye, L. Dynamic Assembly of Molecularly Imprinted Polymer Nanoparticles. *J. Colloid Interf. Sci.* **2018**, *509*, 463-471.